Sensors & Diagnostics

COMMUNICATION

Check for updates

Simple and fast detection of CD4 and CD8 cells: integration of image flow system and acoustophoresis

Enjian Jin, Anna Go and Min-Ho Lee (iD) *

We developed a compact image-based flow cytometry system that combines acoustic focusing with machine learning-driven image analysis. The system enables rapid detection of stained CD4 and CD8 cells flowing on an acoustically defined focal plane, without the need for hydrodynamic focusing. This design allows for a compact configuration while maintaining reliable performance and reduced complexity, making the system suitable for both clinical diagnostics and point-of-care applications.

Flow cytometry (FCM) is widely employed to characterize individual biological cells in motion by simultaneously measuring their scattering and fluorescence with high speed and sensitivity.[1] With its advances in technology, FCM enables the measurement of cell size, internal structure, and functions, and it can distinguish cells of interest with extremely high speed.[1,2] This capability is facilitated by a flow cell that aligns cells into a single stream at high speed, along with a multi-detection optical system capable of capturing multiple fluorescent signals and the corresponding scattering signals at a high data acquisition rate.[2] Due to their effective detection capabilities, many FCM systems continue to utilize expensive and complex optical configurations, which include high-powered lasers to excite 4–5 fluorescent labels and multiple photodetectors for quantifying emissions from different biomarker labels.[3] This advanced detection capability still necessitates the use of costly and intricate optical systems and compensation processes in most FCMs.[4] In addition, the complexity of interpreting results is compounded using planar graphs such as 2D scatter plots and histograms, which sometimes creates unnecessary artifacts resulting in hindering cell counting.[5,6]

Image flow cytometry (IFCM), which integrates microscopy with traditional flow,[7] represents a significant advancement enabling the observation of both cell morphologies and functional characteristics of targeted cells. This technology has shown its potential for detailed analysis in samples containing a wide range of cell types. Various studies obtaining simultaneous acquisitions of thousands of cell images in an ultrafast way and with high detection sensitivity have been performed by applying the optimization of optical modules for the generation of light sheet planes.[8–10]

The fundamental detection system of IFCMs, with some exceptions, has largely remained unchanged, relying on conventional modules such as sheath flow, micro-sized flow channels, high powered multiple lasers, and sCMOS cameras. Such requirements prolong alignment, increase costs, and slow down image analysis.[11–14]

Recently, high-throughput analysis of images of targeting analytes could be obtained with the use of geometry designs of microfluidic channels,[9,15] integration with acoustic force[10] and optimization of imaging.[16] In addition, integration with other detection methodologies other than optical label based detection were performed.[9,17]

In this study, we present a generalized approach to optical flow cytometry that integrates acoustophoresis technology with image-based analysis for the detection, counting, and characterization of CD4 and CD8 cells in flow. The custom-built system is capable of detecting three labeled fluorescence signals while simultaneously monitoring flowing cells or equivalent particles in bright field. By utilizing acoustic standing waves, the system vertically localizes cells onto the focal plane within a microfluidic channel, achieving optical focusing without the need for a sheath flow device. This configuration enables continuous monitoring and imaging of cells or particles in flow using a 10× objective lens, thereby making the system compact and cost-effective.

A piezo ceramic transducer (PZT) was attached to one side of the microfluidic channel wall, and the microfluidic channel was fabricated to have a half wavelength, generating an acoustic standing wave pressure node. The concept of node generation in flow is well-documented in the existing literature.[18,19]

School of Integrative Engineering, Chung-Ang University, 84 Heukseok-ro, Dongjak-Gu, Seoul 06974, Republic of Korea. E-mail: mhlee7@cau.ac.kr

In general, the governing equation for focusing particles is presented in eqn (1), where F_{rad} represents axial radiation force, a is the particle radius, E represents averaged acoustic energy density, Φ is the acoustic contrast factor, k is $2\pi f/c_0$, with f as the frequency, d is the particle position in the wave propagation, c_p and c_0 are the speeds of sound in the material and fluid, and ρ_p and ρ_0 are the densities of the particle and fluid, respectively. From the equation, we could see that the focusing conditions are mostly dependent on the particle size and density.

$$F_{rad} = 4\pi a^3 kE \sin(2kd)\Phi, \qquad (1)$$

where,

$$\Phi = \frac{\rho_o + \frac{2}{3}\left(\rho_p - \rho_0\right)}{2\rho_p + \rho_0} - \frac{1}{3}\frac{\rho_c c_0^2}{\rho_c c_p^2}$$

$$E = \frac{P_0^2}{4\rho_0 c_0^2}$$

Fig. 1 shows the schematic of an overall process for performing experiments for this study. The process begins with the pretreatment of samples, which includes WBC separation, dilution, and staining. The diluted and stained WBCs were then loaded into the acoustic fluidic chip using a syringe pump. The flowing WBCs were spatially positioned toward the focal plane and then captured using an AI-based image capture program, stored, and analyzed. The captured images of stained cells with CD markers and fluorescence were automatically segmented and then defined by an image basis analysis as is depicted in the SI Material section. To obtain clinically meaningful results, it is essential to quantify CD4 and CD8 cells. Accordingly, the ability to capture and analyse many CD4 and CD8 cells within the field of view of the optical system is critical. In this study, the developed optical system enabled high-throughput image acquisition of cells or equivalent particles in flow, providing sufficient data for subsequent analysis using an image processing algorithm. The implemented algorithm performs cells and particle detection, segmentation, and classification, thereby facilitating accurate identification and enumeration of cell populations.

All solvents and stock solutions were prepared with deionized water with a resistance not less than 18.2 MΩ cm. The microspheres for calibration were purchased from Spherotech (URCP-100-2) and fluorescent microspheres for quantification were purchased from Bangs laboratories, Inc. Three types of microspheres were used (Dragon Green, Suncast Yellow, Flash Red) and each has 480/520, 540/600, and 660/690 nm, respectively for excitation and emission wavelengths. Their sizes were measured to be approximately 7.32 um. Phosphate-buffered saline at pH 7.4 was acquired from Thermo Fisher Scientific.

The staining antibodies CD4-BB515 (BD Horizon™ BB515 Mouse Anti-Human CD4, Cat No. 564420), CD3, 19, 56-PE (BD Pharmingen™ PE Mouse Anti-Human CD3, 19, 56 Cat No. 566684, 561741, 556647), CD8-APC (BD Pharmingen™ APC Mouse Anti-Human CD8, Cat No. 561952) and lyze C buffer (BD FACS™ Lysing Solution, Cat No. 349202) were obtained from BD Biosciences, USA.

All these experiments were conducted in the fabricated microchannel which is described in the SI section.

Fig. 2 illustrates the schematic of the optical flow cytometry system developed for this study. A prototype multi-wavelength flow cytometer was constructed by Aligned Genetics (Anyang, Korea). This developed optical flow cytometry is capable of simultaneously capturing bright-field images and detecting fluorescence emissions at three distinct wavelengths, thereby enabling multi-parameter analysis of WBCs stained with different fluorescence markers.

A compact, low-power laser module (FISBA, λ = 488/520/638 nm, 30 mW) was integrated to efficiently excite the fluorescent dyes while maintaining compatibility with bright field imaging. The laser beams were directed at a 30-degree angle relative to the microchannel sensing region, where flowing WBCs were sequentially illuminated by both the LED and laser sources. The emitted fluorescence signals from each stained WBC were collected through an objective lens (Olympus UPLFN 10×, NA 0.3), passed through a slit and a notch filter, and subsequently separated by a series of dichroic mirrors with cut-off wavelengths of 490 nm, 566 nm, and 650 nm, respectively.
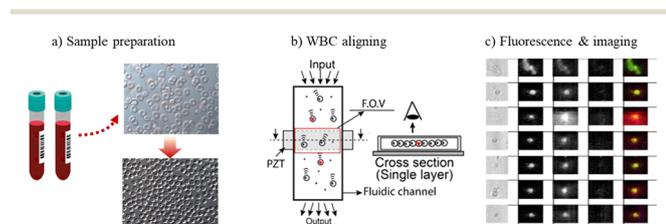

Fig. 1 Step by step preparation of cells. a) Sample preparation (centrifugation and staining), b) WBC aligning in optical focusing plane using the acoustic energy in microscopic channel, and c) fluorescence and image analysis.
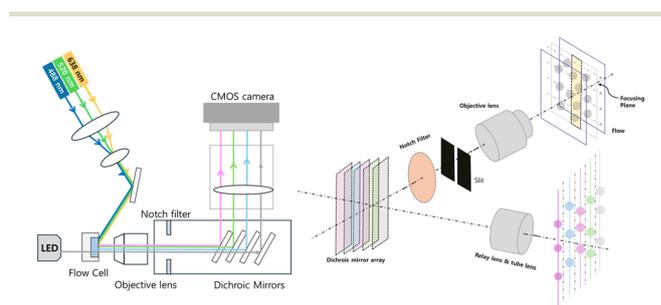

Fig. 2 Schematic of the optical setup for the detection of fluorescence and bright field image. Three focused lasers (wavelengths: 488, 520, 638 nm) pass through a lens to obliquely excite the microfluidic channel. The light then passes through an object lens and selectively through dichroic mirror arrays with cut-off wavelengths of 490 nm, 566 nm, and 650 nm.

This configuration allowed for the selective detection of WBCs labelled with antibodies conjugated to three distinct fluorescent dyes corresponding to the excitation wavelengths.

Both the emitted fluorescence signals and the transmitted bright-field images were collected by a 10× objective (Plan Fluor 10×, NA 0.3; Nikon, Zurich, Switzerland) and passed through a stack of dichroic mirrors projected on the sensor of a CMOS camera (ace2R, Germany, BASLER AG), enabling integrated image acquisition for downstream analysis.

In detail, the emitted light was directed toward four stacked dichroic mirrors, where it was sequentially separated into four distinct wavelength bands and projected onto the CMOS camera. Each dichroic mirror was tilted by approximately 5° relative to the optical axis, allowing the wavelength-filtered images to be spatially separated and simultaneously captured on the CMOS sensor area ($H \times V$, 6.7 × 5.6 mm^2). As a result, fluorescence signals from particles or white blood cells were recorded in four designated regions of the CMOS sensor corresponding to the bright field, PE, BB515, and APC channels.

The microfluidic module was placed on an *XY* translational stage (Thorlabs, USA) mounted on a custom-built optical module. The cell suspension was loaded in a 1 mL syringe (Gastight, Hamilton Laboratory Products, NV, USA) and delivered at a flow rate of 100 μL min^{-1} with a syringe pump (Zaber linear stage, Vancouver, Canada).

For the detection calibration of the optical system, the formation of optically focal planes driven by the acoustic waves was conducted (Fig. S2). Both polystyrene beads and WBCs in flow were clearly visible when the acoustic waves were applied. In addition, six peak calibrations were performed for the classification of particle sizes at a flow speed of 7 μL min^{-1}, an acoustic frequency of 2.7 MHz, a frame rate of 120 fps, and an exposure time of 7 ms. The fluorescent microspheres used in this study – Dragon Green, Suncast Yellow, Flash Red – have excitation and emission wavelengths of 480/520 nm, 540/600 nm, and 660/690 nm, respectively. These microspheres were diluted using a 0.01% PBST solution. Mixtures of active microspheres with different wavelengths were prepared to assess the reliability of accuracy, precision, and counting based on the measured fluorescence results. As is shown in Fig. S3, six distinct peaks were clearly visible based on their fluorescence intensities. The flow rate was 7 μL min^{-1}, the frequency and applied voltage for the acoustophoresis was 2.7 MHz and 14.8 V$_{pp}$, and the frame rate for the image capture was 120 fps.

Prior to conducting experiments with clinical samples, the Institutional Review Board and Research Ethics Committees of Korea University Guro Hospital (KUGH, IRB No. 2022GR0504) reviewed and approved the assay protocol, amendments, and consent procedures. Clinical serum samples were obtained from KUGH, Seoul, South Korea, following ethical approval. The samples were prepared and separated using centrifugation for subsequent analysis with the developed system, as described in the previous section. The separated clinical white blood cell (WBC) samples were stained with CD4-BB515, Lymphocyte-PE, and CD8-APC, followed by red blood cell lysis and phosphate-

buffered saline (PBS) washing to ensure proper sample preparation for analysis. The overall process for staining protocol is as follows. 200 μL of each standard solution (each diluted 1 : 1000) was prepared. To this, 20 μL of CD4-BB515, Lympo-PE and CD8-APC were added, and the mixture was incubated at room temperature for 15 minutes in the dark to prevent photobleaching. Following the staining step, 1000 μL of OptiLyse-C was added for red blood cell (RBC) lysis, and the sample was incubated at room temperature for 10 minutes.

Subsequently, 6000 μL of phosphate-buffered saline (PBS) was added, and the sample was centrifuged at 2000 rpm for 5 minutes. The supernatant was carefully removed, and the cell pellet was resuspended in 3000 μL of PBS. Finally, each prepared sample was loaded into a syringe for flow cytometric analysis. Through the system optimization, including intensity control of the optical source and gain adjustments, biological markers were selected for the efficient detection of white blood cells (WBCs).

The developed optical system consistently captured flowing stained WBCs and displayed their fluorescence signals according to each label. Fig. 3(a) shows the bright field (BF), PE (red fluorescence, RF), BB515 (green fluorescence, GF), and Cy5 (APC) images of flowing WBCs, together with their corresponding binary images for each label. Fig. 3(b) presents the automatically generated overlaid images in which the different fluorescence signals are combined and displayed in distinct colors.

The developed optical flow system can extract and measure the intensity of multiple fluorescence signals directly from captured images without the need of a photodetector and subsequent signal processing units in contrast to the conventional flow cytometry system.

The overall annotation process was described in the SI section and is shown in Fig. S4. The automated annotation results were then compared with the results obtained from a commercially available optical microscopy-based cytometer (CELENA-X) to evaluate performance and accuracy.
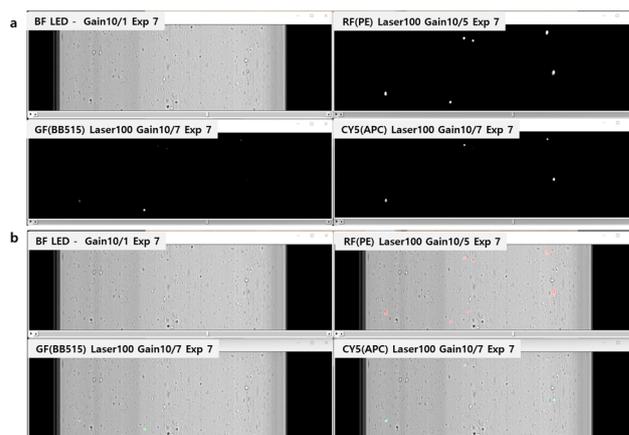

Fig. 3 (a) Bright field and fluorescence images of flowing WBCs, together with their corresponding binary images for each fluorescence label (PE, BB515, and Cy5). (b) Automatically generated overlaid images showing WBCs with distinct colors according to their antibody-specific labeling.
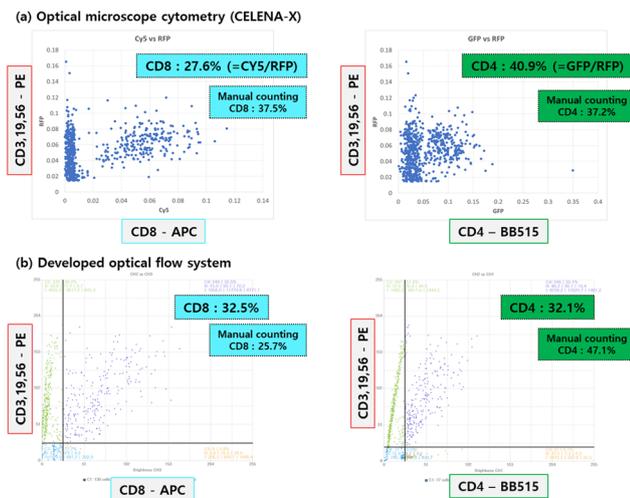
Fig. 4 Classification results of CD4 and CD8 cells. (a) Results obtained using a commercial optical microscopy-based flow cytometry and (b) the corresponding results obtained from the developed optical flow system.

As shown in Fig. 4, the CELENA system identified CD8 and CD4 populations at 27.6% and 40.9% of total WBCs, compared with manual counting values of 37.5% and 37.2%, respectively. Similarly, our system detected CD8 and CD4 populations at 32.5% and 32.1%, while manual counting yielded 25.7% and 47.1%. Although discrepancies were observed, these differences primarily reflect the distinct characteristics of the two approaches: our system acquires high-throughput data from a continuously flowing stream of cells, whereas the reference method relies on a fixed and limited set of stationary images. This methodological distinction highlights the advantage of our system in analyzing a substantially larger number of cells within a short time, thereby enhancing statistical robustness despite small variations in individual measurements.

Conclusions

In this study, we developed an acoustic-based optical flow cytometry system integrated with a flow cell. To minimize reliance on manual analysis, we incorporated a machine learning-driven image capture algorithm, enabling automatic segmentation and quantitative analysis of the extracted image data. The image-based analysis automatically measured the fluorescence intensities of flowing particles and WBCs through wavelength-specific filter sections.

Clinical validation showed slight discrepancies compared with results obtained from optical microscopy. These differences were mainly attributed to manually controlled sample preparation steps, such as washing and red blood cell lysis. We anticipate that with the adoption of automated and precisely controlled sample preparation, the system is expected to achieve performance comparable to conventional microscopy, thereby enhancing reliability and clinical applicability.

Taken together, these results demonstrate the feasibility of combining acoustic focusing with image-based cytometry

for compact, cost-effective, and label-specific cell analysis. With further refinement, including integration of automated sample preparation and high-throughput analysis modules, this platform has strong potential as a next-generation tool for clinical diagnostics and point-of-care testing

Author contributions

Enjian Jin: methodology, investigation, data curation, formal analysis, visualization, and writing. Anna Go: visualization, writing, formal analysis, and methodology. Min-Ho Lee: writing, funding acquisition, project administration, supervision, review & editing.

Conflicts of interest

There are no conflicts to declare.

Data availability

The data supporting this article have been included as part of the supplementary information (SI).

Supplementary information is available. See DOI: **https://doi.org/10.1039/d5sd00108k**.

Acknowledgements

References

1   K. M. McKinnon, *Curr. Protoc. Immunol.*, 2018, **120**, 5.1–5.11.
2   S. Holmberg-Thyden, K. Grønbæk, A. Ortved Gang, D. E. Fassi and S. R. Hadrup, *Anal. Biochem.*, 2021, **627**, 114210.
3   K. M. Mckinnon, *Methods Mol. Biol.*, 2018, **1678**, 139–150.
4   I. P. Sugar, J. Gonzales-Lergier and S. C. Sealfon, *Cytometry, Part A*, 2011, **79**, 356–360.
5   R. Garcia-Varela, R. M. Garcia-Garcia, B. A. Barba-Davila, O. Fajardo, S. O. Serna-Saldivar and G. A. Cardineau, *Molecules*, 2015, **20**, 18685–18703.
6   V. S. Donnenberg and A. D. Donnenberg, *Methods*, 2015, **82**, 3–11.
7   K. Goda, A. Ayazi, D. R. Gossett, J. Sadasivam, C. K. Lonappan, E. Sollier, A. M. Fard, S. C. Hur, J. Adam, C. Murray, C. Wang, N. Brackbill, D. Di Carlo and B. Jalali, *Proc. Natl. Acad. Sci. U. S. A.*, 2012, **109**(29), 11630–11635.
8   T. Miura, H. Mikami, A. Isozaki, T. Ito, Y. Ozeki and K. Goda, *Biomed. Opt. Express*, 2018, **9**, 3424–3433.

9   G. Holzner, B. Mateescu, D. V. Leeuwen, G. Cereghetti, R. Dechant, S. Stavrakis and A. deMello, *Cell Rep.*, 2021, **34**, 108824.

10 M. Ugawa and S. Ota, *Small Sci.*, 2022, **2**, 2100126.

11 Y. Han and Y.-H. Lo, *Sci. Rep.*, 2015, **5**, 13267.

12 E. J. Gualda, H. Pereira, G. G. Martins, R. Gardner and N. Moreno, *Cytometry, Part A*, 2017, **91**, 144–151.

13 P. Rees, H. D. Summers, A. Filby, A. E. Carpenter and M. Doan, *Nat. Rev. Methods Primers*, 2022, **2**, 86.

14 V. A. Russack and R. L. Artymyshyn, *Crit. Rev. Clin. Lab. Sci.*, 1994, **31**, 1–34.

15 T. Miura, H. Mikami, A. Isozaki, T. Ito, Y. Ozeki and K. Goda, *Biomed. Opt. Express*, 2018, **9**, 3424–3433.

16 A. S. Rane, J. Rutkauskaite, A. deMello and S. Stavrakis, *Chem*, 2017, **3**, 588–602.

17 M. Lindley, J. G. d. Pablo, W. Peterson, A. Isozaki, K. Hiramatsu and K. Goda, *Adv. Mater. Technol.*, 2022, **7**, 2101567.

18 F. Petersson, A. Nilsson, C. Holm, H. Jönsson and T. Laurell, *Lab Chip*, 2005, **5**, 20–22.

19 A. Lenshof, C. Magnusson and T. Laurell, *Lab Chip*, 2012, **12**, 1210–1223.